First Measurement of Atmospheric Mercury Species in Qomolangma Nature Preserve, Tibetan Plateau, and Evidence of Transboundary Pollutant Invasion

Authors

Huiming Lin[1], Yindong Tong[2*], Xiufeng Yin[3,4,5], Qianggong Zhang[4,6], Hui Zhang[7], Haoran Zhang[1], Long Chen[8], Shichang Kang[3,5,6], Wei Zhang[9], James Schauer[10,11], Benjamin de Foy[12], Xiaoge Bu[2], Xuejun Wang[1**]

Affiliations

1. MOE Laboratory of Earth Surface Processes, College of Urban and Environmental Sciences, Peking University, Beijing, 100871, China;

2. School of Environmental Science and Engineering, Tianjin University, Tianjin, 300072, China;

3. State Key Laboratory of Cryospheric Science, Northwest Institute of Eco-Environment and Resources, Chinese Academy of Sciences, Lanzhou, 730000, China;

4. Key Laboratory of Tibetan Environment Changes and Land Surface Processes, Institute of Tibetan Plateau Research, Chinese Academy of Sciences, Beijing, 100101, China;

5. University of Chinese Academy of Sciences, Beijing, 100039, China;

6. CAS Center for Excellence in Tibetan Plateau Earth Sciences, Beijing, 100085, China;

7. State Key Laboratory of Environmental Geochemistry, Institute of Geochemistry, Chinese Academy of Sciences, Guiyang, 550002, China;

8. School of Geographic Sciences, East China Normal University, Shanghai, 200241, China;

9. School of Environment and Natural Resources, Renmin University of China, Beijing, 100872, China;

10. Department of Civil and Environmental Engineering, University of Wisconsin-Madison, WI, 53706, USA;

11. Wisconsin State Laboratory of Hygiene, University of Wisconsin-Madison, WI, 53706, USA;

12. Department of Earth and Atmospheric Sciences, Saint Louis University, MO, 63108, USA;

Correspondence:

*Yindong Tong, Tianjin University, Tianjin, China, Email at: yindongtong@tju.edu.cn;

**Xuejun Wang, Peking University, Beijing, China, Email at: wangxuejun@pku.edu.cn;

Abstract

Located in the world's 'Third Pole' and a remote region connecting the Indian Ocean plate and the Eurasian plate, Qomolangma National Nature Preserve (QNNP) is an ideal region to study the long-range transport of atmospheric pollutants. In this study, gaseous elemental mercury (GEM), gaseous oxidized mercury (GOM) and particle-bound mercury (PBM) were continuously measured during the Indian monsoon transition period in QNNP. A slight increase in GEM concentration was observed from the preceding the Indian Summer Monsoon period (1.31±0.42 ng m^{-3}) to the Indian Summer Monsoon period (1.44±0.36 ng m^{-3}), while significant decreases were observed in GOM and PBM concentrations, with concentrations decreasing from 35.2±18.6 to 19.3±10.9 pg m^{-3} ($p<0.001$) for GOM and from 30.5±12.5 to 24.9±19.8 pg m^{-3} ($p<0.001$) for PBM. A unique daily pattern of GEM concentration in QNNP was observed, with a peak value before sunrise and a low value at noon. Relative to the low GEM concentrations, GOM concentrations (with a mean value of 21.4±13.4 pg m^{-3}, n=1239) in this region were relatively high compared with the measured values in some other regions of China. A cluster analysis indicated that the air masses transported to QNNP changed significantly at different stages of the monsoon, and the major potential Hg sources shifted from north India and west Nepal to east Nepal and Bangladesh. Because there is a large area covered in glaciers in QNNP, local glacier winds could increase transboundary transport of pollutants and transport polluted air masses to the Tibetan Plateau. The atmospheric Hg concentration in QNNP in the Indian Summer Monsoon period was influenced by transboundary Hg flows. This sets forth the need for a more specific identification of Hg sources impacting QNNP and underscores the importance of international cooperation for global Hg controls.

Keywords

Indian summer monsoon; atmospheric mercury; trans-boundary transport; glacier winds; Qomolangma National Nature Preserve

1. Introduction

Understanding atmospheric mercury (Hg) concentrations in remote regions is vital to understand the global atmospheric Hg cycling processes (Zhang et al., 2016a;Angot

et al., 2016;AMAP/UNEP, 2013). Generally, atmospheric Hg can be divided into three major types: gaseous elemental Hg (GEM), gaseous oxidized Hg (GOM) and particle-bound Hg (PBM) (Selin, 2009). Over 95% of atmospheric Hg exists in the form of GEM (Ebinghaus et al., 2002;Huang et al., 2014). Due to its stable chemical properties and long lifetime in the atmosphere (approximately 0.3 to 1 year), GEM can be transported over long distances (Horowitz et al., 2017;Travnikov et al., 2017;Selin, 2009). In contrast, GOM and PBM could deposit quickly from the atmosphere, exposing local environments to significant impacts (Lindberg and Stratton, 1998;Seigneur et al., 2006;Lynam et al., 2014). To understand the global and regional cycling of atmospheric Hg, different Hg monitoring networks and sites have been established in recent decades, such as the Atmospheric Mercury Network (AMNet) (Gay et al., 2013) and Global Mercury Observation System (GMOS), which contains over 40 ground-based monitoring stations distributed in the world (Sprovieri et al., 2016). Generally, atmospheric Hg background concentrations range between 1.5 to 1.7 in the northern hemisphere and 1.1 to 1.3 ng m^{-3} in the southern hemisphere (Lindberg et al., 2007;Slemr et al., 2015;Venter et al., 2015;Sprovieri et al., 2016). However, existing studies are still far from sufficient to obtain a full understanding of long-range Hg transport because of insufficient monitoring data in remote and less-populated regions (Zhang et al., 2015a;Fu et al., 2012a).

The trans-boundary and long-range transport of pollutants have attracted considerable attentions in the northeastern and southeastern regions of the Tibetan Plateau (Yang et al., 2018;Li et al., 2016;Zhang et al., 2015b;Pokhrel et al., 2016). The transboundary flows of atmospheric pollutants to the Tibetan Plateau have been identified for pollutants such as persistent organic pollutants and black carbon (Yang et al., 2018;Li et al., 2016;Zhang et al., 2015b;Pokhrel et al., 2016). It was reported that smoke from biomass burning in the Indian subcontinent could pass over natural barrier of the Himalaya (Wang et al., 2015;Pokhrel et al., 2016). HCHs, DDTs and PCBs were all found to have their highest concentrations in the southeast Tibetan Plateau during the monsoon season (Wang et al., 2018). Similar conditions have also occurred for black carbon (Li et al., 2016). However, studies of the trans-boundary transport of Hg on the

Tibetan Plateau are still limited. The existing Hg monitoring data is affected to varying extents by local emission sources (Fu et al., 2012a; Zhang et al., 2015; Zhang et al., 2016). Fu et al. (2012a) report that air masses with high Hg concentrations passed over the urban and industrial areas in Western China and Northern India, and influenced the atmospheric Hg concentrations in Waliguan on the northeastern edge of the Tibetan Plateau. At Shangri-La, located on the southeastern edge of the Tibetan Plateau, the atmospheric Hg sources were reported to be Southeast Asia, India and mainland China (Zhang et al., 2015a). Nevertheless, studies are still lacking on trans-boundary transport of Hg in the Qomolangma National Nature Preserve (QNNP), which directly connects the Indian Subcontinent and Eurasia. The detailed pollutant transport pathways and seasonal or daily patterns of atmospheric Hg concentrations in this region are still not clear.

QNNP, located on the southern edge of the Tibetan Plateau, is considered one of the world's cleanest regions (Qiu, 2008). With an average altitude of ~4,500 m a.s.l., QNNP is a remote region with sparse human population and rare industries (Qiu, 2008; Yao et al., 2012b; Li et al., 2016). However, it is surrounded by two large potential pollution sources: the populated and developed eastern China region, which has experienced about 30 years of rapid industrial development, and South Asian developing countries (e.g., India, Nepal, and Bangladesh), which have also been developing rapidly in recent years (Streets et al., 2011;Zhang et al., 2015b;Yang et al., 2018). China and India are reported as the largest coal consumers in the world (BP Statistical Review of World Energy 2018), and coal combustion is the largest source of atmospheric Hg emissions globally, accounting for ~86% of Hg emissions (Chen et al., 2016a). China is predicted to become the largest economy in the world in the next 20-50 years, and India is predicted to catch up with the Euro area before 2030 (Pacyna et al., 2016). The rapidly growing economies have led to rapid increases in energy demands and hence increasing domestic Hg emissions (Pacyna et al., 2016). With the implementation of control strategies, the atmospheric Hg emissions is forecasted to be about 242 tonnes in China in 2020 (Wu et al., 2018). However, atmospheric Hg emissions in India are expected to increase to about 540 tonnes Hg by 2020 (Burger Chakraborty et al., 2013). Because

QNNP is located on the pathway of air mass transport due to the Indian Summer Monsoon (ISM) (Li et al., 2016), meteorological conditions in QNNP vary significantly during the monsoon transition period (Wang et al., 2001). The monthly average precipitation can range from less than 50 mm in the non-ISM period to 950 mm in the ISM period (Panthi et al., 2015). In addition to the monsoon, the glacial coverage in QNNP is approximately 2,710 km^2 (Nie et al., 2010). Glacier winds could therefore have direct effects on the local pollutant transport because downslope glacier winds can transport polluted air from the upper levels to the land surface (Cai et al., 2007). The atmosphere in QNNP is therefore vulnerable to surrounding pollution sources (Li et al., 2016;Xu et al., 2009).

To the best of our knowledge, the present work is the first study regarding Hg monitoring and source identification in the QNNP covering both the period preceding the Indian Summer Monsoon (PISM) and during the Indian Summer Monsoon (ISM). We performed continuous measurements of GEM, GOM and PBM concentrations for 2 weeks during the onset of the monsoon and for 3.5 months during the monsoon itself. To identify the detailed sources, we combined the real-time Hg monitoring data with a backward trajectory analysis, clustering analysis and potential source contribution function (PSCF) analysis. We further discuss the effects of local glacier winds, caused by the large spatial extent of QNNP glaciers, on the trans-boundary transport of pollutants. This combined monitoring and modeling study could help researchers and government managers to better understand the global Hg cycling processes and potential impacts from the rapidly developing countries in South Asia on the atmospheric Hg concentrations in QNNP.

2. Materials and methods

2.1 Atmospheric Hg monitoring site

Atmospheric Hg monitoring was conducted at the “Atmospheric and Environmental Comprehensive Observation and Research Station, Chinese Academy of Sciences on Mt. Qomolangma” (latitude: 28°21’54” N, longitude: 86°56’53” E) in QNNP, at an altitude of 4,276 m a.s.l. (Figure 1). In QNNP, Mt. Qomolangma spreads from east to the west along the border between the Indian subcontinent and the Tibetan Plateau

(Figure 1). Due to its high altitude, QNNP is naturally isolated from the populated regions, and only rare local Hg emission sources have been observed (AMAP/UNEP, 2013). The most populated region near this monitoring site is Tingri County (with a population density of 4 persons per km^2), located ~40 km to the southwest of the monitoring site. The average annual temperature is 2.1 °C and the total annual rainfall is 270.5 mm in QNNP (Chen et al., 2016b). QNNP is located along the air mass transport pathway of the ISM (Li et al., 2016), and the meteorological conditions in QNNP have significant variations between the PISM and ISM periods (Wang et al., 2001). During the transition period, the temperature in the Tibetan Plateau and South Asia changes from "southern warm - northern cool" to "northern warm - southern cool" (Wang et al., 2001). This reversal leads to a significant increase of diabatic heating over South Asia and the southern slope of the Tibetan Plateau (Ge et al., 2017), which further affects the wind directions and speeds. Local glacier winds could also affect the transport of air masses in QNNP. Glaciers cover ~2,710 km^2 in QNNP (Nie et al., 2010), and most of the glaciers are located on the northern slope of the mountain (Figure 1) (Bolch et al., 2012). The glacier wind is a continuous downslope wind blowing from glacier surfaces down to the foothills of the mountain throughout the day. Hence, the transport of air masses in this region is a combination of atmospheric circulation (monsoon) and local weather conditions (glacier winds). The structure of the boundary layer over QNNP is also significantly affected by glaciers (Li et al., 2006). The height of the atmospheric boundary layer follows a diurnal profile ranging from ~350 m above ground level during the night to ~2000 m during the day (Li et al., 2006).

2.2 GEM, GOM and PBM monitoring

To describe the changes of atmospheric Hg concentrations during the PISM and ISM periods, real-time continuous measurements of GEM, GOM and PBM concentrations were carried out using the Tekran 2537B, 1130 and 1135 instruments (Tekran Inc., Toronto, Canada) from 15 April, 2016 to 14 August, 2016. During the operation of the Tekran instruments, ambient air was introduced into the instrument for 60 minutes through an impactor, a KCL-coated annular denuder, and a Quartz Fiber Filter (QFF). All the Hg species were converted into Hg(0) and then measured by cold vapor atomic

fluorescence spectroscopy (CVAFS). The collected PBM and GOM were desorbed in succession to Hg(0) at the temperature of 800 °C and 500 °C, respectively. Hg-free air was used to flush the 1130 and 1135 systems to introduce the desorbed PBM and GOM into model 2537B for analysis. The GEM was collected at 5-minutes intervals. The sampling inlet was set at ~1.5 m above the instrument platform (shown in Figure S1). To mitigate the impacts of low atmospheric pressures on the pump's train, a low air sampling rate of 7 L min^{-1} for the pump model and 0.75 L min^{-1} (at a standard pressure of 1013 hPa and temperature of 273.14 K) for model 2537B was applied (Swartzendruber et al., 2009;Zhang et al., 2015a;Zhang et al., 2016a). The Tekran 2537B analyzer was calibrated automatically using the internal Hg permeation source inside the instrument every 23 h, and the internal source was calibrated before and after the monitoring by an external Hg source using a syringe. The Tekran ambient Hg analyzer has been described in more details in the previous publications (Landis et al., 2002;Rutter et al., 2008;de Foy et al., 2016). Recent studies have suggested that there may be a low bias of GOM and PBM concentrations for small sample loads of Hg(e.g. less than 10 pg) (Slemr et al., 2016;Ambrose, 2017). Hence, the monitoring data with GOM or PBM concentrations below 23.8 pg m^{-3} were recalculated by the method of Slemr et al. (2016). The updated GOM concentrations increased slightly from 21.3±13.5 pg m^{-3} to 21.4±13.4 pg m^{-3} and from 25.5±19.2 pg m^{-3} to 25.6±19.1 pg m^{-3} for PBM.

2.3 Meteorological data

Throughout the sampling period, the meteorological information was recorded using the Vantage Pro2 weather station (Davis Instruments, USA) with a 5-minute resolution. The monitored parameters included the temperature (with a precision of 0.1°C), relative humidity (with a precision of 1%), wind speed (with a precision of 0.1 m s^{-1}), wind direction (with a precision of 1°), air pressure (with a precision of 0.1 hPa), solar radiation (with a precision of 1 W m^{-2}) and UV index (with a precision of 0.1 MEDs). The snow cover data was obtained from the Moderate Resolution Imaging Spectroradiometer (MODIS) instrument on board the Terra and Aqua satellites (MOD10A1, Hall et al., 2010) with a daily 0.05° resolution.

2.4 Backward trajectory simulation

To identify the atmospheric Hg sources, the Hybrid Single-Particle Lagrangian Integrated Trajectory (HYSPLIT) model was applied to perform a backward trajectory simulation (Stein et al., 2015;Chai et al., 2016;Chai et al., 2017;Hurst and Davis, 2017). The HYSPLIT model, known as a complete and mature system for modeling air parcel trajectories of complex pollutant dispersion and deposition, was developed by the US National Oceanic and Atmospheric Administration (NOAA). Global Data Assimilation System (GDAS) data with 1°×1° latitude and longitude horizontal spatial resolution and 23 vertical levels at 6-hour intervals was used for the backward trajectory simulation. All the trajectory arrival heights were set to 1000 m above ground level. Every backward trajectory was simulated for 72 hours in 6-hour intervals, and the air mass transport regions covered China, Nepal, India, Pakistan and majority of west Asia. Backward trajectories during the whole monitoring period were calculated, and cluster analysis was carried out to identify the Hg transport pathways. The cluster statistics summarize the percentage of back trajectories in each cluster, and the average GEM concentrations are linked with each cluster. The clustering algorithm utilized in this study is based on Ward's hierarchical method (Ward Jr, 1963), which minimizes angular distances between corresponding coordinates of the individual trajectories. By averaging similar or identical pathways from existing air mass pathways to the receptor site, clusters can help identify the mean transport pathways of air masses and provide the primary directions of pollutants transported to the measurement site.

The Potential Source Contribution Function (PSCF) model is a hybrid receptor model using the calculated backward trajectories to estimate the contributions of different emission sources in upwind regions and has been applied in many previous studies (Kaiser et al., 2007;Fu et al., 2012b;Kim et al., 2005;Zhang et al., 2013). The PSCF calculation is made based on counting the trajectory segments that terminate within each cell to determine the values for the grid cells in the study domain (Ashbaugh et al., 1985). In this study, the PSCF model was used to identify the possible sources of atmospheric GEM. The study domain was separated as i × j cells. Then, the PSCF value for the ij^{th} cell is defined as follows:

$$PSCF_{ij} = \frac{M_{ij}}{N_{ij}}$$

where N_{ij} is the total number of endpoints that fall into ij^{th} cell during the whole simulation period, and M_{ij} is the number of endpoints for the same cell that correspond to GEM concentrations higher than a set criterion. In this study, PSCF values were calculated based on the average GEM concentration during the whole sampling campaign. The PSCF value stands for the conditional probability that the GEM concentration at the measurement site is larger than the average GEM concentration if the parcel passes through the ij^{th} cell before it reaches the measurement site.

To account for and reduce the uncertainty due to low values of N_{ij}, the PSCF values were scaled by an arbitrary weighting function W_{ij} (Polissar et al., 1999). While the total number of the endpoints in a cell (N_{ij}) is less than ~three times the average value of the end points for each cell, the weighting function will decrease the PSCF values. In this study, W_{ij} was set using the following piecewise function:

$$W_{ij} = \begin{cases} 1.00 & N_{ij} > 3\,N_{ave} \\ 0.70 & 3\,N_{ave} > N_{ij} > 1.5N_{ave} \\ 0.42 & 1.5N_{ave} > N_{ij} > N_{ave} \\ 0.05 & N_{ave} > N_{ij} \end{cases}$$

We used the PSCF analysis to evalutate the effects of biomass burning regions using the MODIS fire data. MODIS fire spots data from 1 April 2016 to 31 August 2016 was obtained from the Fire Information for Resource Management System (FIRMS) operated by the National Aeronautics and Space Administration (NASA) of the United States (Giglio et al., 2003; Davies et al., 2004).

3. Results and discussion

3.1 Comparisons of atmospheric Hg concentrations between PISM and ISM

The GEM, GOM and PBM concentrations at the sampling site were 1.42±0.37 ng m^{-3} (n=15180), 21.4±13.4 pg m^{-3} (n=1239) and 25.6±19.1 pg m^{-3} (n=1237), respectively, during the whole study period (Figure 2 and Table 1). GEM accounted for over 95% of all the atmospheric Hg species. Figure S2 shows a comparison of the GEM, GOM and PBM concentrations during the PISM and ISM periods. During the PISM period, the average GEM, GOM and PBM concentrations were 1.31±0.42 ng m^{-3} (n=2001),

35.2±18.6 pg m^{-3} (n=167), and 30.5±12.5 pg m^{-3} (n=168), respectively, while during the ISM period, the average GEM, GOM and PBM concentrations were 1.44±0.36 ng m^{-3} (n=13179), 19.3±10.9 pg m^{-3} (n=1072), and 24.9±19.8 pg m^{-3} (n=1069), respectively. The concentrations of GEM, GOM and PBM are statistically significant different ($p<0.001$) between PISM and ISM period. We further compared the Hg concentrations at different ISM stages. Figure S2 shows that GEM concentrations increased significantly with the development of ISM ($p<0.001$ between ISM1 and ISM4), while decreases of GOM and PBM concentrations were observed during the study period ($p<0.001$ between ISM1 and ISM5), with decreases of 37.9% (from 20.3±7.38 pg m^{-3} to 12.6±8.82 pg m^{-3}) and 48.1% (from 21.2±7.38 pg m^{-3} to 11.0±5.85 pg m^{-3}), respectively. Reason for the higher PBM concentrations during ISM2 is discussed in Section 3.3.2.

Table 2 summarizes GEM, GOM and PBM concentrations and diurnal variations of GEM measured by the Tekran system in some previous studies in Asia. Generally, the GEM concentration in the QNNP was approaching the reported values in the Northern Hemisphere (~1.5 to 1.7 ng m^{-3}) and was higher than those in the Southern Hemisphere (~1.1 to 1.3 ng m^{-3}) (Lindberg et al., 2007;Slemr et al., 2015;Venter et al., 2015;Sprovieri et al., 2016). Among the global Hg monitoring sites, the EvK2CNR monitoring site on the southern slope of the Tibetan Plateau, Nepal, is the nearest station (at a straight-line distance of approximately 50 km) from the monitoring site in this study (Gratz et al., 2013). The average GEM concentration at EvK2CNR (1.2±0.2 ng m^{-3}, from Nov. 2011-Apr. 2012) was slightly lower than that in the QNNP (1.31±0.42 ng m^{-3} during the PISM period and 1.44±0.36 ng m^{-3} during the ISM period). Compared with the Hg concentration in Nam Co station (Yin et al., 2018) in the central Tibetan plateau (1.33±0.24 ng m^{-3}), the GEM concentration in QNNP was higher during the ISM period. Compared with Hg concentrations observed at China's background stations and rural regions (e.g., Waliguan Baseline Observatory (1.98±0.98 ng m^{-3}) (Fu et al., 2012a), Ailaoshan Mountain National Natural Reserve (2.09±0.63 ng m^{-3}) (Zhang et al., 2016a), and Shangri-La Baseline Observatory in Yunnan province (2.55±0.73 ng m^{-3}) (Zhang et al., 2015a)), the average GEM concentration in the QNNP was lower.

However, despite its low GEM concentration, GOM concentration (with a value of 21.4±13.4 pg m^{-3}) in QNNP was relatively high compared with the values in the clean regions (usually lower than 10 pg m^{-3}, Table 2) or even some polluted regions of China (such as the suburban area of Beijing (10.1±18.8 pg m^{-3}), Shanghai (21±100 pg m^{-3})) (Zhang et al., 2013;Duan et al., 2017) (Table 2). One possible explanation for the high GOM concentration is the strong subsidence in QNNP. The subsidence of the free troposphere would bring GOM-enriched air masses to the surface layer (Faïn et al., 2009), resulting in the observed high surface GOM levels (Weiss- Penzias et al., 2009). In QNNP, with the wide distribution of glaciers, glacier winds could bring the upper air masses to the land surface layer (Song et al., 2007), which could further strengthen the subsidence movement. Low wet deposition rate of GOM caused by the rare precipitation in QNNP (~270mm) (Chen et al., 2016c) could be another reason for the high GOM concentrations (Prestbo and Gay, 2009).

The increases of GEM concentrations during the ISM period could indicate the impacts of trans-boundary transport, which has been confirmed by previous studies (Fu et al., 2012a;Zhang et al., 2016a). The deposition of GEM from the atmosphere to the land surface is difficult, and GEM has a much longer residence time than the other Hg species (Horowitz et al., 2017;Travnikov et al., 2017;Selin, 2009). At Ailaoshan in Yunnan province (Zhang et al., 2016a), a higher TGM concentration during the ISM period (2.22±0.58 ng m^{-3}) than the PISM period (1.99±0.66 ng m^{-3}) was also observed. The TGM concentration during the ISM period (2.00±0.77 ng m^{-3}) was also higher than that during the PISM period (1.83±0.78 ng m^{-3}) at Waliguan station in the northeastern Tibetan Plateau (Fu et al., 2012a). In contrast to GEM, the GOM and PBM levels during the ISM period were lower than the monitored values during the PISM period (Figure S2 and Table 2). In previous studies, the PBM concentration in the Kathmandu Valley was lower during the monsoon period (with a value of 120.5±105.9 pg m^{-3}) than the pre-monsoon (with a value of 1855.4±780.8 pg m^{-3}) and post-monsoon period (with a value of 237.6±199.4 pg m^{-3}) (Guo et al., 2017). In India, PBM concentrations during the monsoon period (with a value of 158±34 pg m^{-3}) were lower than those in the non-monsoon season (with a value of 231±51 pg m^{-3}) (Das et al., 2016). This fact could be

possibly attributed to precipitation increases brought by the monsoon, which further causes wet depositions of PBM from atmosphere. During the ISM period, the precipitation could increase by up to 25% in the South Asia and Tibetan Plateau (Ji et al., 2011).

3.2 Diurnal variation of atmospheric Hg species in QNNP

During the PISM period, all the atmospheric Hg species showed clear diurnal patterns (Figure 3 and Figure S3). For GEM, the minimum concentrations usually occurred at ~12 p.m. (0.84±0.11 ng m^{-3}, UTC +6 time), while maximum values occurred before dawn (1.98±0.51 ng m^{-3} at ~5:30 a.m.). During the afternoon, GEM concentration increased consistently and reached a peak at sunrise (with a value of 1.98 ng m^{-3}). Unlike the daily GEM changes, GOM and PBM concentrations usually reached maximum concentrations from ~10:00 a.m. to ~4:00 p.m. in the day, and the concentrations remained relative stable for the rest of the day. During the ISM period, the diurnal variation of atmospheric Hg species was less pronounced compared to the values in the PISM period. At different stages of the ISM period, the diurnal pattern was also different. The GEM diurnal variation value (peak value minus lowest value in the same period) decreased over time, from 1.03 ng m^{-3} during the initial ISM period to 0.43 ng m^{-3} during the final ISM period. For GEM concentrations during the ISM period, the minimum values all occurred at ~2:00 p.m., and the maximum values were observed at ~6:00 a.m. After sunrise, GEM concentrations decreased continuously to lower values at noon.

Compared with diurnal profiles of GEM from previous studies, the diurnal tendency in QNNP is unique (shown in Table 2). For the sampling sites in other studies, the highest GEM concentrations were usually observed during the daytime (Nair et al., 2012;Fu et al., 2008;Mukherjee et al., 2009;Karthik et al., 2017;Jen et al., 2014). Kellerhals et al. (2003) reported that the majority of monitoring sites in CAMNet have a common pattern with the maximum concentrations around noon and minimum concentrations before sunrise. Compared to other observation stations and considering QNNP as a remote region with high altitude, sparse population and rare industries, the observed results here may indicate a simple mechanism of variation in GEM

concentration without the complex effect of human activities. Previous studies suggested that the planetary boundary layer (PBL) could have significant effects on the concentrations of atmospheric pollutants near the ground (Han et al., 2009;Tie et al., 2007;Quan et al., 2013). With a large glacier coverage (~2,710 km^2), the structure of the boundary layer over QNNP was significantly affected by glacier winds (Li et al., 2006). The local PBL may be subject to impacts from the glacier-covered environment and have a significant diurnal variation. The height of the atmospheric boundary layer could vary significantly from ~350 m above ground level to ~2000 m in one day (Li et al., 2006). Following sunrise, with the strengthening of the glacier wind, a strong convection current starts to grow in the troposphere, and the stock of GEM in the near-ground atmosphere is depleted quickly, leading to the quick decrease in concentrations. In contrast, after sunset, with the weakening of the glacier wind, the nocturnal stable boundary layer takes a dominate position controlling the surface layer, and its height is relatively low (Li et al., 2006), which could lead to increases in GEM concentrations.

Comparing the diurnal variations between the PISM and ISM period, the atmospheric Hg concentrations have almost the same pattern of variations. However, the magnitude of the variation during the ISM period is lower relative to the PISM period, and the variation becomes even smaller in the later stages of the ISM (Figure 3). The GEM concentration usually peaked at ~5 a.m. - 6 a.m. in both PISM and ISM periods. While the peak GEM concentrations were almost at the same level in the whole period, the decreasing diurnal variations were mainly due to the increasing GEM concentrations in the afternoon. The increased GEM concentrations in the afternoon may indicate new GEM sources in the ISM period. One possible source of GEM in the afternoon might be Hg(0) reemission from the glaciers. Holmes et al. (2010) reported that snow-covered land could be a reservoir for the conversion of oxidized Hg to Hg(0) under sunlight, and approximately 60% of the Hg deposited to snow cover could eventually be reemitted to the air. A shorter reservoir lifetime for deposited Hg in snowpack was also reported when temperature rises (Faïn et al., 2007). With the increase of ambient temperature and radiation from April to August, the reemission of GEM from the glaciers could increase as well. As the snow coverage in the QNNP decreased

significantly from the PISM to the ISM period (Figure S4), some of the released Hg may become a source of new GEM from the initial ISM to the final stage of the ISM period. More Hg(0) could be released due to the higher temperature and stronger radiation in the afternoon. However, some other factors such as changes in the PBL heights and in wind directions could also be partly responsible for the diurnal variations of GEM concentrations (Horowitz et al., 2017;Travnikov et al., 2017;Selin, 2009;Li et al., 2006).

3.3 Source identification for atmospheric Hg in the QNNP

3.3.1 Wind direction dependence of Hg concentrations

Figure 4 shows the concentration roses of GEM, GOM and PBM at the sampling site during the PISM and ISM period, respectively. All concentrations of the three species have a strong dependence on the wind directions. During the PISM period, the predominant wind directions with Hg masses are northeast and southwest. Wind from the northeast of QNNP originates from and/or passes through other parts of China. The southwest wind, which is the dominant direction and contains the largest amount of Hg, potentially brought air masses from India and Nepal to QNNP. During the ISM period, the predominant wind directions with Hg changed to the south and northeast. Considering the transport rates of species Hg concentrations (length of sector) from different directions, both directions may have greatly contributed to the Hg concentration in QNNP, while the air masses from south brought relatively larger amounts of GOM and PBM.

Relatively low GEM concentrations (<1.5 ng m^{-3}) were observed in most of the samples (80.0%) of air masses in the predominant Hg-transport direction (from southwest to west) during the PISM period, which is due to the control of westerlies. With high wind speeds (Table 1) and coming from Central Asia, the westerlies are the predominant wind containing low pollutant levels that spread in the QNNP during the PISM period (Kotlia et al., 2015). Relatively high GEM concentrations (>1.5 ng m^{-3}) were found in 92.4% of the samples for the predominant Hg direction during the ISM period under the control of the monsoon (Kotlia et al., 2015), which might indicate that the transported air masses are coming from polluted regions. GOM and PBM had

similar patterns under the control of the westerlies and monsoon during the PISM and ISM period, respectively.

3.3.2 Air mass back trajectories analysis

To further quantify the contributions of different sources to GEM concentrations, an air mass back trajectory simulation and trajectory cluster analyses were applied in this study. Figure 5 provides the trajectory clusters of GEM during the PISM and ISM periods. According to the total spatial variation index, all the trajectories in different periods were grouped into 3-6 clusters. During the PISM period (Figure 5a), GEM concentration from cluster 1 (with a frequency of 12%) was the highest (1.32 ng m^{-3}), which originated from or passed through central Asia and northern India. Cluster 2 (30%) and cluster 4 (17%) represent air masses that pass through northern India and northwestern Nepal. According to the local Hg emission inventory (AMAP/UNEP, 2013), Hg in this air mass most likely originated from central Pakistan and northern India. Cluster 3 (41%) represents the air masses that originated from or passed through different cities in northern India. Based on the previous atmospheric Hg emission inventories (Simone et al., 2016;AMAP/UNEP, 2013), Hg emissions in west Asia and central Asia are not significant. Based on a combination of the pathway analysis, emission inventory and GEM concentrations during the PISM period, almost all the GEM transported by air masses to QNNP was from northern India and passed through Nepal.

During the ISM period (Figure 5b-5f), the transport pathways of atmospheric Hg changed significantly with the onset of the monsoon and differed strongly from the PISM period. During the ISM1 period (Figure 5b), the onset of the ISM was under development, leading to scattered clusters. GEM levels in cluster 2 (23%) were the highest (1.52 ng m^{-3}), which originated from or passed through the Tibetan Plateau. The high GEM concentrations could possibly result from the Hg emissions from the burning of yak dung (Xiao et al., 2015;Chen et al., 2015;Rhode et al., 2007;Huang et al., 2016). Cluster 1 (17%) and cluster 3 (60%) represent the pollutant coming from Nepal, and the trajectory is relatively short. During the ISM2 period, all the clusters originated from or passed through central Asia, northern India and northwestern Nepal (Figure 5c).

447 The clusters were similar to most of the clusters during PISM period; however, the
448 GEM concentrations in these clusters were higher than those during the PISM period,
449 which might be caused by the large Hg emissions from frequent fires in the source
450 region during ISM2 (Finley et al., 2009) (Figure S5). During the ISM3 period (Figure
451 5d), most of the clusters moved from west to south of QNNP. Cluster 4 (1.56 ng m^{-3},
452 46%) represents the pollutant coming from Bangladesh and passing through
453 southeastern Nepal. Cluster 3 (1.54 ng m^{-3}, 40%) originated from or passed through
454 central Nepal. The share of air masses coming from central Asia, northern India and
455 northwestern Nepal dropped to approximately 14%. During the ISM4 period (Figure
456 5e), the clusters moved further west to Bangladesh and eastern India. Except for cluster
457 1 (5%), the other clusters originated from or passed through Bangladesh, eastern India
458 and northeastern Nepal. The condition during the ISM5 period was almost the same as
459 the ISM4 period: most of the pollutants were coming from Bangladesh and eastern India
460 and passed through southeastern Nepal.
461 PSCF models were also applied to identify potential sources by combining the
462 backward trajectory simulations and Hg monitoring concentrations. Figure 6 shows the
463 regional contributions of GEM emission sources during the PISM period and ISM
464 period (ISM1-5). During the PISM period (Figure 6a), most of the Hg sources were in
465 Pakistan, northern India and central Nepal (Zhang et al., 2015a). The QNNP was most
466 likely impacted by the Hg emissions in Karachi, Lahore (Pakistan), New Delhi, Uttar
467 Pradesh (India), Katmandu and Pokhara (Nepal), all of which are large urban regions
468 with intensive industrial activities. With the development of the ISM, the potential
469 sources gradually shifted from western Nepal to eastern Nepal and Bangladesh (Figure
470 6b-f). The PSCF analysis indicated that the air masses could have transboundary
471 transport events from Pakistan, India, Nepal and Bangladesh to QNNP.
472 Atmospheric Hg clusters during both the PISM and ISM periods indicated that the
473 air masses, which originated from or passed through northern India and Nepal, would
474 make great contributions to the Hg concentration in the QNNP. Northern India and
475 Nepal were also identified as potential source regions for QNNP. Clusters 2-4 of the
476 PISM period represent the air masses from outside China, and they show that over 88%

of the GEM in QNNP was transported from outside China during the PISM period. During ISM2-5 the period, over 95% of the GEM was transported to QNNP from outside China. Meanwhile, the GEM concentration increased by 10% from the PISM to ISM period according to the site monitoring data, indicating the increasing amount of transported GEM. According to the UNEP Hg emission inventory (AMAP/UNEP, 2013), northern India is an important Hg source which might be responsible for the trans-boundary transportation of Hg to China (Figure 5), and the growing emissions in India are related to the rapidly growing economy and increasing usage of fossil fuels (Sharma, 2003). Considering the heavy air pollutions in Nepal (Rupakheti et al., 2017;Forouzanfar et al., 2015) and in Bangladesh (Islam et al., 2015;Rahman et al., 2018;Rana et al., 2016;Mondol et al., 2014), Nepal and Bangladesh might be underestimated Hg source regions in the modeling and should be taken into consideration in further study.

Under the control of the ISM during the ISM2 period, the high PBM concentration may be related to the biomass burning in the source region. According to the PSCF analysis, northern India and Nepal are the potential source regions during the ISM2 period. The source identification by back trajectory simulation and trajectory cluster analyses also indicated that northern India and Nepal are in the air mass transport trajectory that would transport Hg to QNNP. Finley et al. (2009) reported that PBM concentrations could be associated with Hg emissions from wildfire events. One possible cause of the observed high PBM concentration is the frequent fire events that occurred during the ISM2 period in the air masses trajectory. Figure S4 shows the fire hotspots observed by MODIS from April to August 2016. During the ISM2 period, frequent fire hotspots were identified in the source region, and large amounts of PBM may have been released into the atmosphere from biomass burning (Finley et al., 2009). The transport of those air masses with enriched PBM was controlled by the ISM and intensified by glacier winds. The transport of polluted air to QNNP resulted in the outburst of PBM concentration during the ISM2 period. During the PISM period, although the number of fire hotspots was much higher, most of the fire hotspots locations were not in the potential source region (Figure 6a and Figure S4), resulting in

507 the low PBM concentration observed.

508 **3.4 Implications from this study**

509 At a high altitude and located in the deep southern Tibetan Plateau, QNNP is isolated
510 from anthropogenic perturbations and industrial activities, and this area was thought to
511 be shielded from pollutant inputs from South Asia. However, our results show that the
512 Hg concentration in this region is not as low as previously expected. During the whole
513 monitoring period, the highest GEM concentration reached 3.74 ng m^{-3} (with
514 trajectories passing through the north of India), ~2.5 times higher than the average
515 concentration in the Northern Hemisphere (~1.5 to 1.7 ng m^{-3}) (Lindberg et al.,
516 2007;Slemr et al., 2015;Venter et al., 2015). The average GEM concentration in the
517 middle stage of the ISM was 1.56 ng m^{-3}, which is inside the average range of observed
518 Northern Hemisphere GEM concentrations. Compared with the ISM period, the GEM
519 concentrations in the PISM period were significantly lower, with a value of 1.31±0.42
520 ng m^{-3}. This value during PISM is not high compared with other background monitoring
521 data in the Northern Hemisphere.

522 We now recognize that trans-boundary transportation is an important mechanism that
523 can influence Hg distribution in this region. In particular, the air masses transported to
524 QNNP might be primary under the control of mesoscale ISM drivers and intensified by
525 regional glacier winds (Figure 7). From the PISM to ISM periods, the warm center
526 gradually shifts northwestward from low latitudes to the QNNP (Wang et al., 2001;Ge
527 et al., 2017), and the South Asian High moves onto the Tibetan Plateau and maintains
528 a strong upper-level divergence and upward motion. The upward motion makes the air
529 masses cross the high-altitude Himalayan Mountains and move to mainland China (Xu
530 et al., 2009; Bonasoni et al., 2010). During the ISM period, the transboundary transport
531 of atmospheric Hg is strengthened by both monsoon and glacial winds. However, this
532 effect seems to be weaker during the PISM period. The transboundary-transported air
533 masses can be pumped down right after crossing Mt. Qomolangma due to the control
534 of the regionally unique wind transportation mode, the glacier wind. Hence, in addition
535 to the monsoon, the trans-boundary transport of Hg could also be intensified by regional
536 glacier winds, leading to the increases of atmospheric Hg in this region. As showed in

other studies in the northern or eastern Tibetan Plateau, the glacier wind can pump down air masses from upper level to the surface in QNNP (Cai et al., 2007). The pump movement is remarkably efficient at transporting air masses (Zhu et al., 2006), and could bring significant amount of pollutants to QNNP.

In 2013, the Minamata Convention on Mercury was developed to control global Hg pollution. Atmospheric Hg has been reported to have continuously declined (~1–2% y^{-1}) at the monitoring sites in North America and Europe from 1990 to present (Zhang et al., 2016b). Under the Convention, a National Implementation Plan on Mercury Control has been developed in China to fulfill the commitment to control and reduce Hg emissions (World Bank, 2016). Average GEM concentrations in East China decreased from 2.68±1.07 ng m^{-3} in 2014 to 1.60±0.56 ng m^{-3} in 2016 (Tang et al., 2018). According to the recently updated emission inventory in China (Wu et al., 2016), anthropogenic Hg emissions in China reached a peak amount of about 567 tonnes in 2011 and have decreased since then. In 2014, the anthropogenic Hg emissions decreased to 530 tonnes. This was also confirmed in the concentration of plant Hg from a sampling site near QNNP, which recorded the decrease of atmospheric Hg concentrations in Tibet since the year of 2010 (Tong et al., 2016). However, the source identity analysis in QNNP indicates that foreign regions of China were the main contributor responsible for the observed pollutants (accounting for 95% of the whole trajectory during the main ISM period). This result indicates that the Hg concentration in QNNP could hardly benefit from China's efforts toward Hg reductions. South Asian developing countries (e.g., India, Nepal, and Bangladesh) (Streets et al., 2011; Zhang et al., 2015b; Yang et al., 2018) should be the key to controlling atmospheric Hg concentrations in QNNP. Hg emissions in India were estimated to be approximately 310 tonnes in 2010 and are predicted to rise to 540 tonnes in 2020 (Burger Chakraborty et al., 2013). India, Nepal and Bangladesh all have signed the Minamata Convention, however, only the Indian government has ratified the convention so far. It is urgent for those countries to take immediate actions to reduce Hg emissions, which is crucial to reducing atmospheric Hg concentrations in QNNP.

4. Conclusions

A comprehensive investigation of the concentrations, origin and transport of GEM, GOM and PBM was made in QNNP, a remote, high-altitude station located at the boundary between the Indian subcontinent and the Tibetan Plateau and in the transport pathway of the Indian Summer Monsoon from South Asia to the Tibetan Plateau. The average GEM concentration (1.31±0.42 ng m^{-3}) during the PISM period was lower than that during the ISM period (1.44±0.36 ng m^{-3}). The average GOM and PBM concentrations during the PISM period were higher than those during the ISM period, which might be related to the increasing wet depositions during the ISM period. The average GOM concentration was higher than in most rural areas in the US and China. The GEM concentration had a significant diurnal variation pattern in QNNP, with the maximum GEM concentration observed before sunrise and a sharp decrease after sunrise until noon. The magnitude of the diurnal variation declined from April to August, which could be related to the re-emission of Hg from snow cover and change of planetary boundary layer.

According to the backward trajectory analysis and cluster analysis, most of the air masses with high GEM concentrations in QNNP originated from or passed through Bangladesh, northern India and central Nepal. With the PSCF analysis, we found that Pakistan, northern India and Nepal are potential source regions during the PISM period, and Bangladesh, north India, Nepal were identified as outbound potential sources during the ISM period. During the ISM period, the air masses were able to cross the high-altitude Himalayan Mountains with the help of the ISM. Once the air masses passed over the Himalayas, they could be brought into the surface layer and transported to QNNP by the all-day-long downslope glacier wind. Because Hg is easily transported long distances via the atmosphere, the nations in South Asia must work together to develop and apply appropriate pollutant-reduction strategies to reduce atmospheric Hg emissions.

Acknowledgments

This study was funded by the National Natural Science Foundation of China (Grant #41630748, 41501517, 41571130010) and the Natural Science Foundation of Tianjin (Grant #16JCQNJC08300). The authors are grateful to NOAA for providing the

HYSPLIT model and GFS meteorological files, to NASA for providing the MODIS files. We also thank the staffs of the Atmospheric and Environmental Comprehensive Observation and Research Station of Chinese Academy of Sciences on Mt. Qomolangma for field sampling assistance.

References

AMAP/UNEP: Technical Background Report for the Global Mercury Assessment 2013, Arctic Monitoring and Assessment Program, 2013.

Ambrose, J. L.: Improved methods for signal processing in measurements of mercury by Tekran® 2537A and 2537B instruments, Atmospheric Measurement Techniques, 10, 5063-5073, 2017.

Angot, H., Dion, I., Vogel, N., Legrand, M., Magand, O., and Dommergue, A.: Multi-year record of atmospheric mercury at Dumont d'Urville, East Antarctic coast: continental outflow and oceanic influences, Atmospheric Chemistry and Physics, 16, 8265-8279, 2016.

Ashbaugh, L. L., Malm, W. C., and Sadeh, W. Z.: A residence time probability analysis of sulfur concentrations at Grand Canyon National Park, Atmospheric Environment (1967), 19, 1263-1270, 1985.

Bolch, T., Kulkarni, A., Kääb, A., Huggel, C., Paul, F., Cogley, J., Frey, H., Kargel, J. S., Fujita, K., and Scheel, M.: The state and fate of Himalayan glaciers, Science, 336, 310-314, 2012.

Burger Chakraborty, L., Qureshi, A., Vadenbo, C., and Hellweg, S.: Anthropogenic mercury flows in India and impacts of emission controls, Environmental science & technology, 47, 8105-8113, 2013.

Cai, X., Song, Y., Zhu, T., Lin, W., and Kang, L.: Glacier winds in the Rongbuk Valley, north of Mount Everest: 2. Their role in vertical exchange processes, Journal of Geophysical Research: Atmospheres, 112, 2007.

Chai, T., Stein, A., Ngan, F., and Draxler, R.: Inverse modeling with HYSPLIT Lagrangian Dispersion Model-Tests and Evaluation using the Cross Appalachian Tracer Experiment (CAPTEX) data, AGUFM, 2016.

Chai, T., Crawford, A., Stunder, B., Pavolonis, M. J., Draxler, R., and Stein, A.: Improving volcanic ash predictions with the HYSPLIT dispersion model by assimilating MODIS satellite retrievals, Atom. Chem. Phys., 17, 2865-2879, 2017.

Chen, G., Li, J., Chen, B., Wen, C., Yang, Q., Alsaedi, A., and Hayat, T.: An overview of mercury emissions by global fuel combustion: the impact of international trade, Renewable and Sustainable Energy Reviews, 65, 345-355, 2016a.

Chen, P., Kang, S., Bai, J., Sillanpää, M., and Li, C.: Yak dung combustion aerosols in the Tibetan Plateau: Chemical characteristics and influence on the local atmospheric environment, Atmospheric Research, 156, 58-66, 10.1016/j.atmosres.2015.01.001, 2015.

Chen, P., Gao, Y., Lee, A. T., Cering, L., Shi, K., and Clark, S. G.: Human–carnivore coexistence in Qomolangma (Mt. Everest) Nature Reserve, China: Patterns and compensation, Biological conservation, 197, 18-26, 2016b.

Chen, W.-K., Li, T.-C., Sheu, G.-R., Lin, N.-H., Chen, L.-Y., and Yuan, C.-S.: Correlation analysis, transportation mode of atmospheric mercury and criteria air pollutants, with meteorological parameters at two remote sites of mountain and offshore island in Asia, Aerosol Air Qual. Res, 16, 2692-2705, 2016c.

Das, R., Wang, X., Khezri, B., Webster, R. D., Sikdar, P. K., and Datta, S.: Mercury isotopes of atmospheric particle bound mercury for source apportionment study in urban Kolkata, India, Elem Sci Anth, 4, 2016.

de Foy, B., Tong, Y., Yin, X., Zhang, W., Kang, S., Zhang, Q., Zhang, G., Wang, X., and Schauer, J. J.: First field-based atmospheric observation of the reduction of reactive mercury driven by sunlight, Atmos. Environ., 134, 7e39, 2016.

Duan, L., Wang, X., Wang, D., Duan, Y., Cheng, N., and Xiu, G.: Atmospheric mercury speciation in Shanghai, China, Science of the Total Environment, 578, 460-468, 2017.

Ebinghaus, R., Kock, H., Coggins, A., Spain, T., Jennings, S., and, and Temme, C.: Long-term measurements of atmospheric mercury at Mace Head, Irish west coast, between 1995 and 2001, Atmospheric Environment, 36, 5267-5276, 2002.

Faïn, X., Grangeon, S., Bahlmann, E., Fritsche, J., Obrist, D., Dommergue, A., Ferrari, C. P., Cairns, W., Ebinghaus, R., and Barbante, C.: Diurnal production of gaseous mercury in the alpine snowpack before snowmelt, J. Geo. Res. Atmos., 112, 2007.

Faïn, X., Obrist, D., Hallar, A. G., McCubbin, I., and Rahn, T.: High levels of reactive gaseous mercury observed at a high elevation research laboratory in the Rocky Mountains, Atmos. Chem. Phys., 9, 8049-8060, 10.5194/acp-9-8049-2009, 2009.

Feng, X., and Fu, X.: Monsoon-facilitated characteristics and transport of atmospheric mercury at a high-altitude background site in southwestern China, Atmos. Chem. Phys, 1680, 7324, 2016.

Finley, B., Swartzendruber, P., and Jaffe, D.: Particulate mercury emissions in regional wildfire plumes observed at the Mount Bachelor Observatory, Atmospheric Environment, 43, 6074-6083, 2009.

Forouzanfar, M. H., Alexander, L., Anderson, H. R., Bachman, V. F., Biryukov, S., Brauer, M., Burnett, R., Casey, D., Coates, M. M., and Cohen, A.: Global, regional, and national comparative risk assessment of 79 behavioural, environmental and occupational, and metabolic risks or clusters of risks in 188 countries, 1990–2013: a systematic analysis for the Global Burden of Disease Study 2013, The Lancet, 386, 2287-2323, 2015.

Fu, X., Feng, X., Zhu, W., Wang, S., and Lu, J.: Total gaseous mercury concentrations in ambient air in the eastern slope of Mt. Gongga, South-Eastern fringe of the Tibetan plateau, China, Atmospheric Environment, 42, 970-979, 2008.

Fu, X., Feng, X., Dong, Z., Yin, R., Wang, J., Yang, Z., and Zhang, H.: Atmospheric gaseous elemental mercury (GEM) concentrations and mercury depositions at a high-altitude mountain peak in south China, Atmospheric Chemistry and Physics, 10, 2425-2437, 2010.

Fu, X., Feng, X., Liang, P., Zhang, H., Ji, J., and Liu, P.: Temporal trend and sources of speciated atmospheric mercury at Waliguan GAW station, Northwestern China, Atmospheric Chemistry and Physics, 12, 1951-1964, 2012a.

Fu, X., Feng, X., Shang, L., Wang, S., and Zhang, H.: Two years of measurements of atmospheric total gaseous mercury (TGM) at a remote site in Mt. Changbai area, Northeastern China, Atmospheric Chemistry and Physics, 12, 4215-4226, 2012b.

Gay, D. A., Schmeltz, D., Prestbo, E., Olson, M., Sharac, T., and Tordon, R.: The Atmospheric Mercury Network: measurement and initial examination of an ongoing atmospheric mercury record across North America, Atmospheric Chemistry and Physics, 13, 11339-11349, 10.5194/acp-13-11339-2013, 2013.

Ge, J., You, Q., and Zhang, Y.: The influence of the Asian summer monsoon onset on the northward movement of the South Asian high towards the Tibetan Plateau and its thermodynamic mechanism, International Journal of Climatology, 2017.

Global, B. P.: BP statistical review of world energy June 2018, em: http://www.bp.com/en/global/corporate/energy-economics/statistical-review-of-world-energy.html, 2018.

Gratz, L., Esposito, G., Dalla Torre, S., Cofone, F., Pirrone, N., and Sprovieri, F.: First Measurements of Ambient Total Gaseous Mercury (TGM) at the EvK2CNR Pyramid Observatory in Nepal, E3S Web of Conferences, 2013.

Guo, J., Kang, S., Huang, J., Zhang, Q., Rupakheti, M., Sun, S., Tripathee, L., Rupakheti, D., Panday, A. K., and Sillanpää, M.: Characterizations of atmospheric particulate-bound mercury in the Kathmandu Valley of Nepal, South Asia, Sci. Total Environ., 579, 1240-1248, 2017.

Han, S., Bian, H., Tie, X., Xie, Y., Sun, M., and Liu, A.: Impact of nocturnal planetary boundary layer on urban air pollutants: Measurements from a 250-m tower over Tianjin, China, Journal of hazardous materials, 162, 264-269, 2009.

Holmes, C. D., Jacob, D. J., Corbitt, E. S., Mao, J., Yang, X., Talbot, R., and Slemr, F.: Global atmospheric model for mercury including oxidation by bromine atoms, Atmospheric Chemistry and Physics, 10, 12037-12057, 2010.

Horowitz, H. M., Jacob, D. J., Zhang, Y., Dibble, T. S., Slemr, F., Amos, H. M., Schmidt, J. A., Corbitt, E. S., Marais, E. A., and Sunderland, E. M.: A new mechanism for atmospheric mercury redox chemistry: Implications for the global mercury budget, Atmospheric Chemistry and Physics, 17, 6353-6371, 2017.

Huang, J., Lyman, S. N., Hartman, J. S., and Gustin, M. S.: A review of passive sampling systems for ambient air mercury measurements, Environmental science. Processes & impacts, 16, 374-392, 10.1039/c3em00501a, 2014.

Huang, J., Kang, S., Guo, J., Zhang, Q., Cong, Z., Sillanpää, M., Zhang, G., Sun, S., and Tripathee, L.: Atmospheric particulate mercury in Lhasa city, Tibetan Plateau, Atmospheric Environment, 142, 433-441, 2016.

Hurst, T., and Davis, C.: Forecasting volcanic ash deposition using HYSPLIT, Journal of Applied Volcanology, 6, 5, 2017.

Islam, M. F., Majumder, S. S., Al Mamun, A., Khan, M. B., Rahman, M. A., and Salam, A.: Trace metals concentrations at the atmosphere particulate matters in the Southeast Asian Mega City (Dhaka, Bangladesh), Open Journal of Air Pollution, 4, 86, 2015.

Jen, Y.-H., Chen, W.-H., Hung, C.-H., Yuan, C.-S., and Ie, I.-R.: Field measurement of total gaseous mercury and its correlation with meteorological parameters and criteria air pollutants at a coastal site of the Penghu Islands, Aerosol Air Qual. Res, 14, 364-375, 2014.

Ji, Z., Kang, S., Zhang, D., Zhu, C., Wu, J., and Xu, Y.: Simulation of the anthropogenic aerosols over South Asia and their effects on Indian summer monsoon, Climate dynamics, 36, 1633-1647, 2011.

Kaiser, A., Scheifinger, H., Spangl, W., Weiss, A., Gilge, S., Fricke, W., Ries, L., Cemas, D., and Jesenovec, B.: Transport of nitrogen oxides, carbon monoxide and ozone to the alpine global atmosphere watch stations Jungfraujoch (Switzerland), Zugspitze and Hohenpeißenberg (Germany), Sonnblick (Austria) and Mt. Krvavec (Slovenia), Atmospheric Environment, 41, 9273-9287, 2007.

Karthik, R., Paneerselvam, A., Ganguly, D., Hariharan, G., Srinivasalu, S., Purvaja, R., and Ramesh, R.: Temporal variability of atmospheric Total Gaseous Mercury and its correlation with meteorological parameters at a high-altitude station of the South India, Atmospheric Pollution Research, 8, 164-173, 2017.

Kellerhals, M., Beauchamp, S., Belzer, W., Blanchard, P., Froude, F., Harvey, B., McDonald, K., Pilote, M., Poissant, L., and Puckett, K.: Temporal and spatial variability of total gaseous mercury in Canada: results from the Canadian Atmospheric Mercury Measurement Network (CAMNet), Atmospheric Environment, 37, 1003-1011, 2003.

Kim, E., Hopke, P. K., Kenski, D. M., and Koerber, M.: Sources of fine particles in a rural midwestern

US area, Environmental science & technology, 39, 4953-4960, 2005.
Kotlia, B. S., Singh, A. K., Joshi, L. M., and Dhaila, B. S.: Precipitation variability in the Indian Central Himalaya during last ca. 4,000 years inferred from a speleothem record: Impact of Indian Summer Monsoon (ISM) and Westerlies, Quaternary International, 371, 244-253, 2015.
Landis, M. S., Stevens, R. K., Schaedlich, F., and Prestbo, E. M.: Development and characterization of an annular denuder methodology for the measurement of divalent inorganic reactive gaseous mercury in ambient air, Environmental science & technology, 36, 3000-3009, 2002.
Li, C., Bosch, C., Kang, S., Andersson, A., Chen, P., Zhang, Q., Cong, Z., Chen, B., Qin, D., and Gustafsson, Ö.: Sources of black carbon to the Himalayan–Tibetan Plateau glaciers, Nature Communications, 7, 12574, 2016.
Li, M., Dai, Y., Ma, Y., Zhong, L., and Lu, S.: Analysis on structure of atmospheric boundary layer and energy exchange of surface layer over Mount Qomolangma region, Plateau Meteorology, 25, 807-813, 2006.
Lindberg, S., Bullock, R., Ebinghaus, R., Engstrom, D., Feng, X., Fitzgerald, W., Pirrone, N., Prestbo, E., and Seigneur, C.: A synthesis of progress and uncertainties in attributing the sources of mercury in deposition, AMBIO: a Journal of the Human Environment, 36, 19-33, 2007.
Lindberg, S. a., and Stratton, W.: Atmospheric mercury speciation: concentrations and behavior of reactive gaseous mercury in ambient air, Environmental Science & Technology, 32, 49-57, 1998.
Lynam, M. M., Dvonch, J. T., Hall, N. L., Morishita, M., and Barres, J. A.: Spatial patterns in wet and dry deposition of atmospheric mercury and trace elements in central Illinois, USA, Environmental Science and Pollution Research, 21, 4032-4043, 2014.
Mondol, M., Khaled, M., Chamon, A., and Ullah, S.: Trace metal concentration in atmospheric aerosols in some city areas of Bangladesh, Bangladesh Journal of Scientific and Industrial Research, 49, 263-270, 2014.
Mukherjee, A. B., Bhattacharya, P., Sarkar, A., and Zevenhoven, R.: Mercury emissions from industrial sources in India and its effects in the environment, in: Mercury Fate and Transport in the Global Atmosphere, Springer, 81-112, 2009.
Nair, U. S., Wu, Y., Walters, J., Jansen, J., and Edgerton, E. S.: Diurnal and seasonal variation of mercury species at coastal-suburban, urban, and rural sites in the southeastern United States, Atmospheric environment, 47, 499-508, 2012.
Nie, Y., Zhang, Y., Liu, L., and Zhang, J.: Monitoring glacier change based on remote sensing in the Mt. Qomolangma National Nature Preserve, 1976–2006, Acta Geographica Sinica, 65, 13-28, 2010.
Panthi, J., Dahal, P., Shrestha, M. L., Aryal, S., Krakauer, N. Y., Pradhanang, S. M., Lakhankar, T., Jha, A. K., Sharma, M., and Karki, R.: Spatial and temporal variability of rainfall in the Gandaki River Basin of Nepal Himalaya, Climate, 3, 210-226, 2015.
Pokhrel, B., Gong, P., Wang, X., Gao, S., Wang, C., and Yao, T.: Sources and environmental processes of polycyclic aromatic hydrocarbons and mercury along a southern slope of the Central Himalayas, Nepal, Environmental Science and Pollution Research, 23, 13843-13852, 2016.
Polissar, A., Hopke, P., Paatero, P., Kaufmann, Y., Hall, D., Bodhaine, B., Dutton, E., and Harris, J.: The aerosol at Barrow, Alaska: long-term trends and source locations, Atmospheric Environment, 33, 2441-2458, 1999.
Prestbo, E. M., and Gay, D. A.: Wet deposition of mercury in the US and Canada, 1996–2005: Results and analysis of the NADP mercury deposition network (MDN), Atmospheric Environment, 43, 4223-4233, 2009.

771 Qiu, J.: China: the third pole, Nature News, 454, 393-396, 2008.
772 Quan, J., Gao, Y., Zhang, Q., Tie, X., Cao, J., Han, S., Meng, J., Chen, P., and Zhao, D.: Evolution of
773 planetary boundary layer under different weather conditions, and its impact on aerosol concentrations,
774 Particuology, 11, 34-40, 2013.
775 Rahman, M. M., Mahamud, S., and Thurston, G. D.: Recent spatial gradients and time trends in Dhaka,
776 Bangladesh air pollution and their human health implications, Journal of the Air & Waste Management
777 Association, 2018.
778 Rana, M. M., Sulaiman, N., Sivertsen, B., Khan, M. F., and Nasreen, S.: Trends in atmospheric particulate
779 matter in Dhaka, Bangladesh, and the vicinity, Environmental Science and Pollution Research, 23,
780 17393-17403, 2016.
781 Rhode, D., Madsen, D. B., Brantingham, P. J., and Dargye, T.: Yaks, yak dung, and prehistoric human
782 habitation of the Tibetan Plateau, Developments in Quaternary Sciences, 9, 205-224, 2007.
783 Rupakheti, D., Adhikary, B., Praveen, P. S., Rupakheti, M., Kang, S., Mahata, K. S., Naja, M., Zhang,
784 Q., Panday, A. K., and Lawrence, M. G.: Pre-monsoon air quality over Lumbini, a world heritage site
785 along the Himalayan foothills, Atmospheric Chemistry and Physics, 17, 11041-11063, 2017.
786 Rutter, A. P., Schauer, J. J., Lough, G. C., Snyder, D. C., Kolb, C. J., Von Klooster, S., Rudolf, T.,
787 Manolopoulos, H., and Olson, M. L.: A comparison of speciated atmospheric mercury at an urban center
788 and an upwind rural location, Journal of Environmental Monitoring, 10, 102-108, 2008.
789 Seigneur, C., Vijayaraghavan, K., and Lohman, K.: Atmospheric mercury chemistry: Sensitivity of global
790 model simulations to chemical reactions, Journal of Geophysical Research: Atmospheres, 111, 2006.
791 Selin, N. E.: Global biogeochemical cycling of mercury: a review, Annual Review of Environment and
792 Resources, 34, 43-63, 2009.
793 Sharma, D. C.: Concern over mercury pollution in India, in, Elsevier, 2003.
794 Simone, F. D., Gencarelli, C. N., Hedgecock, I. M., and Pirrone, N.: A modeling comparison of mercury
795 deposition from current anthropogenic mercury emission inventories, Environmental science &
796 technology, 50, 5154-5162, 2016.
797 Slemr, F., Angot, H., Dommergue, A., Magand, O., Barret, M., Weigelt, A., Ebinghaus, R., Brunke, E.-
798 G., Pfaffhuber, K. A., and Edwards, G.: Comparison of mercury concentrations measured at several sites
799 in the Southern Hemisphere, Atmospheric Chemistry and Physics, 15, 3125-3133, 2015.
800 Slemr, F., Weigelt, A., Ebinghaus, R., Kock, H. H., Bödewadt, J., Brenninkmeijer, C. A., Rauthe-Schöch,
801 A., Weber, S., Hermann, M., and Becker, J.: Atmospheric mercury measurements onboard the CARIBIC
802 passenger aircraft, Atmospheric Measurement Techniques, 9, 2291-2302, 2016.
803 Song, Y., Zhu, T., Cai, X., Lin, W., and Kang, L.: Glacier winds in the Rongbuk Valley, north of Mount
804 Everest: 1. Meteorological modeling with remote sensing data, Journal of Geophysical Research:
805 Atmospheres, 112, 2007.
806 Sprovieri, F., Pirrone, N., Bencardino, M., D'Amore, F., Carbone, F., Cinnirella, S., Mannarino, V., Landis,
807 M., Ebinghaus, R., and Weigelt, A.: Atmospheric mercury concentrations observed at ground-based
808 monitoring sites globally distributed in the framework of the GMOS network, Atmospheric Chemistry
809 and Physics, 16, 11915-11935, 2016.
810 Stein, A., Draxler, R. R., Rolph, G. D., Stunder, B. J., Cohen, M., and Ngan, F.: NOAA's HYSPLIT
811 atmospheric transport and dispersion modeling system, Bulletin of the American Meteorological Society,
812 96, 2059-2077, 2015.
813 Streets, D. G., Devane, M. K., Lu, Z., Bond, T. C., Sunderland, E. M., and Jacob, D. J.: All-time releases
814 of mercury to the atmosphere from human activities, Environmental science & technology, 45, 10485-

10491, 2011.
Swartzendruber, P., Jaffe, D., and Finley, B.: Improved fluorescence peak integration in the Tekran 2537 for applications with sub-optimal sample loadings, Atmospheric Environment, 43, 3648-3651, 2009.
Tang, Y., Wang, S., Wu, Q., Liu, K., Wang, L., Li, S., Gao, W., Zhang, L., Zheng, H., and Li, Z.: Recent decrease trend of atmospheric mercury concentrations in East China: the influence of anthropogenic emissions, Atom. Chem. Phys., 18, 8279-8291, 2018.
Tie, X., Madronich, S., Li, G., Ying, Z., Zhang, R., Garcia, A. R., Lee-Taylor, J., and Liu, Y.: Characterizations of chemical oxidants in Mexico City: A regional chemical dynamical model (WRF-Chem) study, Atmospheric Environment, 41, 1989-2008, 2007.
Tong, Y., Yin, X., Lin, H., Wang, H., Deng, C., Chen, L., Li, J., Zhang, W., Schauer, J. J., and Kang, S.: Recent Decline of Atmospheric Mercury Recorded by Androsace tapete on the Tibetan Plateau, Environmental science & technology, 50, 13224-13231, 2016.
Travnikov, O., Angot, H., Artaxo, P., Bencardino, M., Bieser, J., D'Amore, F., Dastoor, A., Simone, F. D., Diéguez, M. d. C., and Dommergue, A.: Multi-model study of mercury dispersion in the atmosphere: atmospheric processes and model evaluation, Atmospheric Chemistry and Physics, 17, 5271-5295, 2017.
Venter, A., Beukes, J., Van Zyl, P., Brunke, E.-G., Labuschagne, C., Slemr, F., Ebinghaus, R., and Kock, H.: Statistical exploration of gaseous elemental mercury (GEM) measured at Cape Point from 2007 to 2011, Atmospheric Chemistry and Physics, 15, 10271-10280, 2015.
Wang, B., Wu, R., and Lau, K.: Interannual variability of the Asian summer monsoon: Contrasts between the Indian and the western North Pacific–East Asian monsoons, Journal of climate, 14, 4073-4090, 2001.
Wang, C., Wang, X., Gong, P., and Yao, T.: Long-term trends of atmospheric organochlorine pollutants and polycyclic aromatic hydrocarbons over the southeastern Tibetan Plateau, Sci. Total Environ., 624, 241-249, 2018.
Wang, X., Gong, P., Sheng, J., Joswiak, D. R., and Yao, T.: Long-range atmospheric transport of particulate Polycyclic Aromatic Hydrocarbons and the incursion of aerosols to the southeast Tibetan Plateau, Atmos. Environ., 115, 124-131, 2015.
Ward Jr, J. H.: Hierarchical grouping to optimize an objective function, Journal of the American statistical association, 58, 236-244, 1963.
Weiss- Penzias, P., Gustin, M. S., and Lyman, S. N.: Observations of speciated atmospheric mercury at three sites in Nevada: Evidence for a free tropospheric source of reactive gaseous mercury, J. Geo. Res. Atmos., 114, 2009.
Wu, Q., Wang, S., Li, G., Liang, S., Lin, C.-J., Wang, Y., Cai, S., Liu, K., and Hao, J.: Temporal trend and spatial distribution of speciated atmospheric mercury emissions in China during 1978–2014, Environmental science & technology, 50, 13428-13435, 2016.
Wu, Q., Li, G., Wang, S., Liu, K., and Hao, J.: Mitigation options of atmospheric Hg emissions in China, Environmental science & technology, 52, 12368-12375, 2018.
Xiao, Q., Saikawa, E., Yokelson, R. J., Chen, P., Li, C., and Kang, S.: Indoor air pollution from burning yak dung as a household fuel in Tibet, Atmospheric Environment, 102, 406-412, 10.1016/j.atmosenv.2014.11.060, 2015.
Xu, B., Cao, J., Hansen, J., Yao, T., Joswia, D. R., Wang, N., Wu, G., Wang, M., Zhao, H., and Yang, W.: Black soot and the survival of Tibetan glaciers, Proceedings of the National Academy of Sciences, 106, 22114-22118, 2009.
Yang, J., Kang, S., Ji, Z., and Chen, D.: Modeling the origin of anthropogenic black carbon and its climatic effect over the Tibetan Plateau and surrounding regions, J. Geo. Res. Atmos., 123, 671-692,

2018.
Yin, X., Kang, S., Foy, B. d., Ma, Y., Tong, Y., Zhang, W., Wang, X., Zhang, G., and Zhang, Q.: Multi-year monitoring of atmospheric total gaseous mercury at a remote high-altitude site (Nam Co, 4730 m asl) in the inland Tibetan Plateau region, Atmospheric Chemistry and Physics, 18, 10557-10574, 2018.
Zhang, H., Fu, X., Lin, C., Wang, X., and Feng, X.: Observation and analysis of speciated atmospheric mercury in Shangri-La, Tibetan Plateau, China, Atmos. Chem. Phys, 15, 653-665, 2015a.
Zhang, H., Fu, X., Lin, C.-J., Shang, L., Zhang, Y., Feng, X., and Lin, C.: Monsoon-facilitated characteristics and transport of atmospheric mercury at a high-altitude background site in southwestern China, Atmospheric Chemistry & Physics, 16, 2016a.
Zhang, L., Wang, S., Wang, L., and Hao, J.: Atmospheric mercury concentration and chemical speciation at a rural site in Beijing, China: implications of mercury emission sources, Atmospheric Chemistry and Physics, 13, 10505-10516, 2013.
Zhang, R., Wang, H., Qian, Y., Rasch, P. J., Easter, R. C., Ma, P.-L., Singh, B., Huang, J., and Fu, Q.: Quantifying sources, transport, deposition, and radiative forcing of black carbon over the Himalayas and Tibetan Plateau, Atom. Chem. Phys., 15, 6205-6223, 2015b.
Zhang, Y., Jacob, D. J., Horowitz, H. M., Chen, L., Amos, H. M., Krabbenhoft, D. P., Slemr, F., Louis, V. L. S., and Sunderland, E. M.: Observed decrease in atmospheric mercury explained by global decline in anthropogenic emissions, Proceedings of the National Academy of Sciences, 113, 526-531, 2016b.
Zhu, T., Lin, W., Song, Y., Cai, X., Zou, H., Kang, L., Zhou, L., and Akimoto, H.: Downward transport of ozone- rich air near Mt. Everest, Geophysical Research Letters, 33, 2006.

Figure captions

Figure 1. Location of Qomolangma National Nature Preserve (QNNP). The red star shows the location of the monitoring station in QNNP. The red dots show the locations of two largest cities in Tibet (Lhasa and Xigaze), with the scale bars showing their distances from the QNNP.

Figure 2. Time series change of GEM, GOM and PBM concentration during the study period. The time series was split into a Pre-Indian Summer Monsoon (PISM) period (15 April-30 April, 2016) and 5 Indian Summer Monsoon (ISM) periods (1 May–12 May (ISM1), 13 May–4 June (ISM2), 5 June–20 June (ISM3), 21 June–10 July (ISM4), 11 July–14 August (ISM5)).

Figure 3. Diurnal variations of GEM, GOM and PBM concentrations during the Pre-Indian Summer Monsoon (PISM) period (15 April–30 April, 2016) and 5 Indian Summer Monsoon (ISM) periods (1 May–12 May (ISM1), 13 May–4 June (ISM2), 5 June–20 June (ISM3), 21 June–10 July (ISM4), 11 July–14 August (ISM5)). The concentrations represent the daily average values during each period.

Figure 4. Concentration roses of GEM, GOM and PBM from different wind directions. The length of each spoke describes the frequency of flow from the corresponding direction.

Figure 5. Clusters of the Back trajectories analysis from the Qomolangma National Nature Preserve (QNNP) monitoring site during the Pre-Indian Summer Monsoon (PISM) period and the 5 Indian Summer Monsoon (ISM) periods. The cluster statistics summarize the percentage of back trajectories for each cluster. The background color shading represents the global Hg emissions from anthropogenic sources (AMAP/UNEP, 2013).

Figure 6. Potential source regions and pathways of GEM using the Potential Source Contribution Function (PSCF) method before and during the Indian Summer Monsoon (ISM). PSCF values represent the probability that a grid cell is a source of Hg.

Figure 7. Conceptual map of transboundary transport of atmospheric Hg in the Himalaya region. Arrows show the impacts of the Indian Summer Monsoon, upward winds and glacial winds on the transboundary transport of Hg.

Figure 1

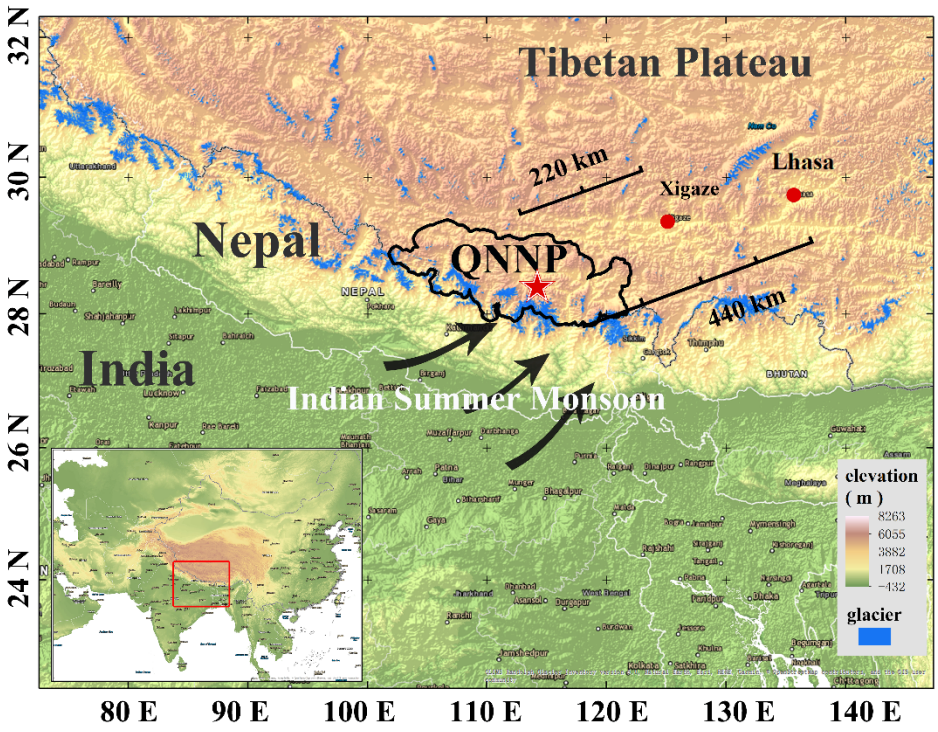
Tibetan Plateau
220 km
Xigaze
Lhasa
Nepal
QNNP
NEPAL
440 km
India
BHUTAN
Indian Summer Monsoon
elevation
(m)
8263
6055
3882
1708
−432
glacier
32 N
30 N
28 N
26 N
24 N
80 E
90 E
100 E
110 E
120 E
130 E
140 E

913 **Figure 2**

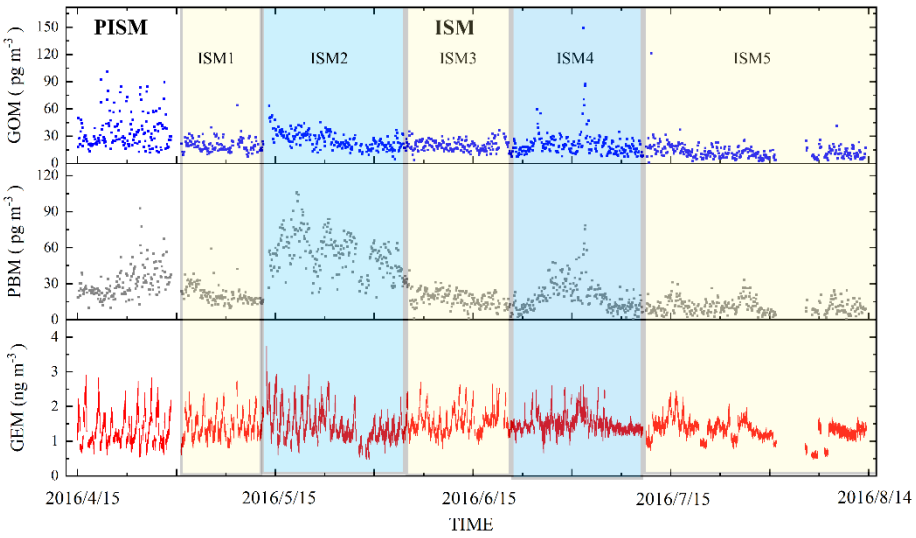

914

915

Figure 3


PISM period
Ism1 period
Ism2 period
Ism3 period
Ism4 period
Ism5 period
Solar Radiation (W m-2)
Wind Speed (m s-1)
Relative Humidity
Wind Direction
GOM (pg m-3)
PBM (pg m-3)
GEM (ng m-3)

Figure 4

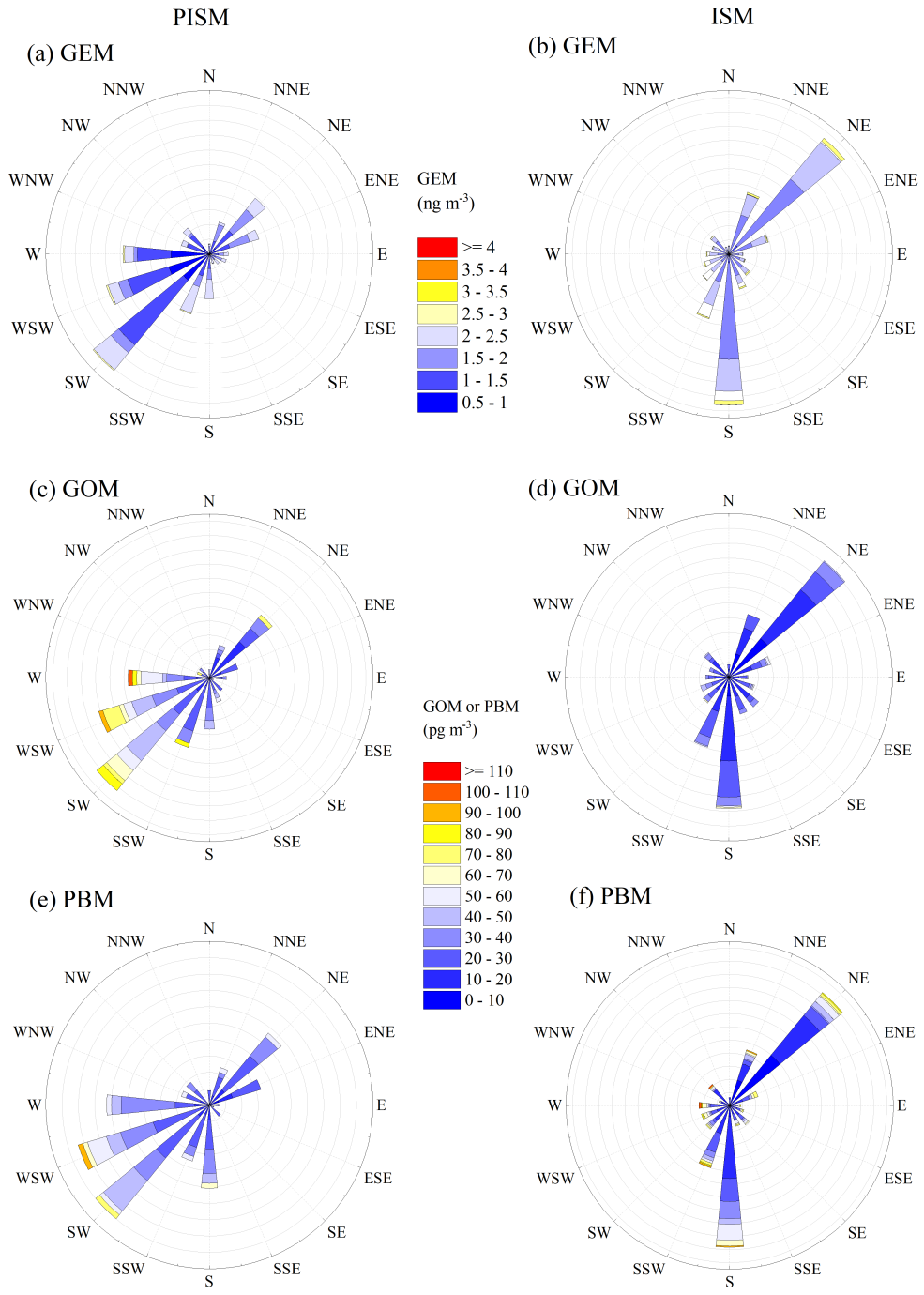
PISM
ISM
(a) GEM
(b) GEM
(c) GOM
(d) GOM
(e) PBM
(f) PBM
N
NNE
NE
ENE
E
ESE
SE
SSE
S
SSW
SW
WSW
W
WNW
NW
NNW
GEM (ng m-3)
>= 4
3.5 - 4
3 - 3.5
2.5 - 3
2 - 2.5
1.5 - 2
1 - 1.5
0.5 - 1
GOM or PBM (pg m-3)
>= 110
100 - 110
90 - 100
80 - 90
70 - 80
60 - 70
50 - 60
40 - 50
30 - 40
20 - 30
10 - 20
0 - 10

Figure 5

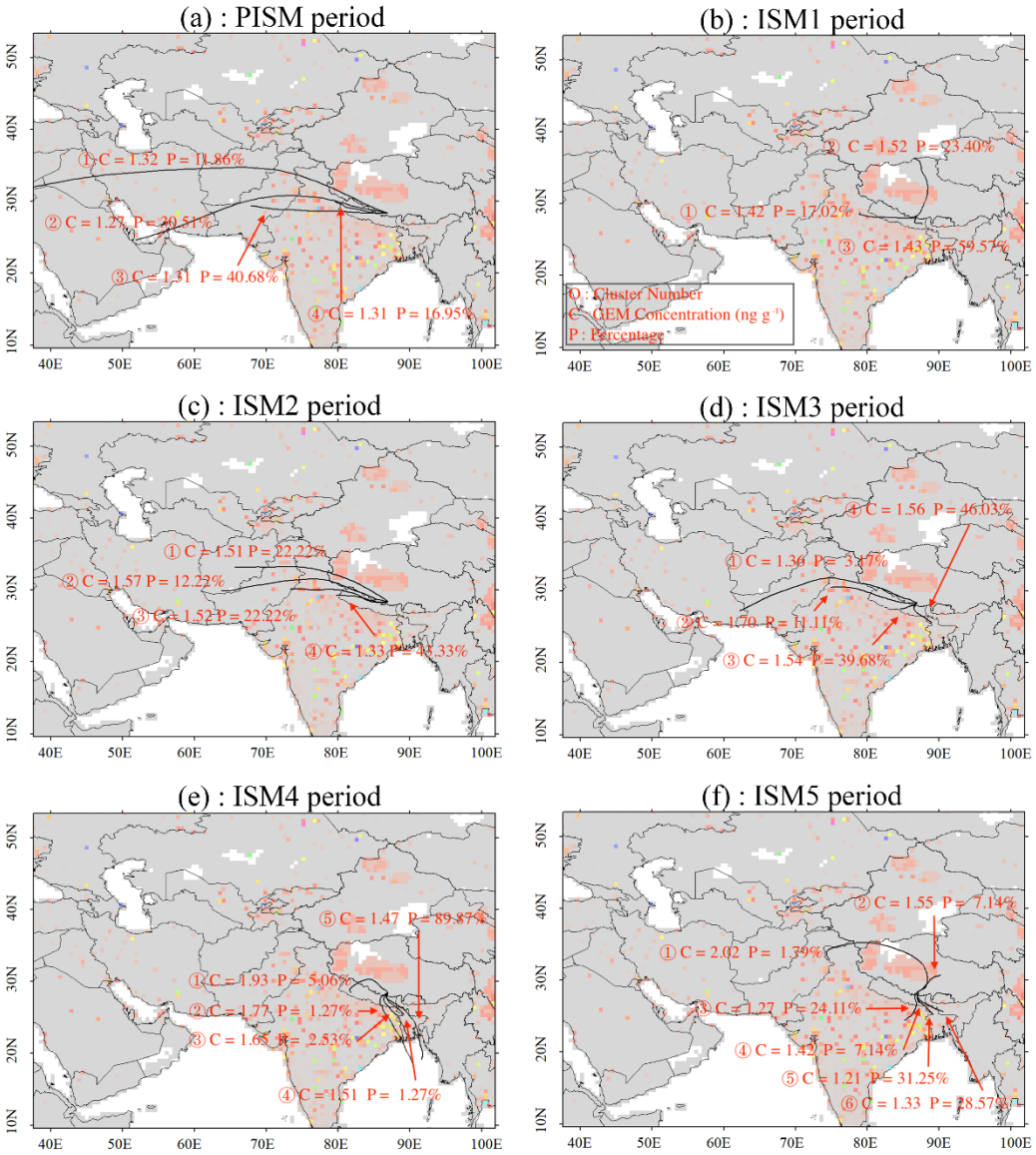
(a) : PISM period
① C = 1.32 P = 11.86%
② C = 1.27 P = 30.51%
③ C = 1.31 P = 40.68%
④ C = 1.31 P = 16.95%
(b) : ISM1 period
② C = 1.52 P = 23.40%
① C = 1.42 P = 17.02%
③ C = 1.43 P = 59.57%
O : Cluster Number
C : GEM Concentration (ng g-1)
P : Percentage
(c) : ISM2 period
① C = 1.51 P = 22.22%
② C = 1.57 P = 12.22%
③ C = 1.52 P = 22.22%
④ C = 1.33 P = 43.33%
(d) : ISM3 period
④ C = 1.56 P = 46.03%
① C = 1.36 P = 3.17%
② C = 1.70 P = 11.11%
③ C = 1.54 P = 39.68%
(e) : ISM4 period
⑤ C = 1.47 P = 89.87%
① C = 1.93 P = 5.06%
② C = 1.77 P = 1.27%
③ C = 1.65 P = 2.53%
④ C = 1.51 P = 1.27%
(f) : ISM5 period
② C = 1.55 P = 7.14%
① C = 2.02 P = 1.59%
③ C = 1.27 P = 24.11%
④ C = 1.42 P = 7.14%
⑤ C = 1.21 P = 31.25%
⑥ C = 1.33 P = 28.57%
50N
40N
30N
20N
10N
40E
50E
60E
70E
80E
90E
100E

Figure 6

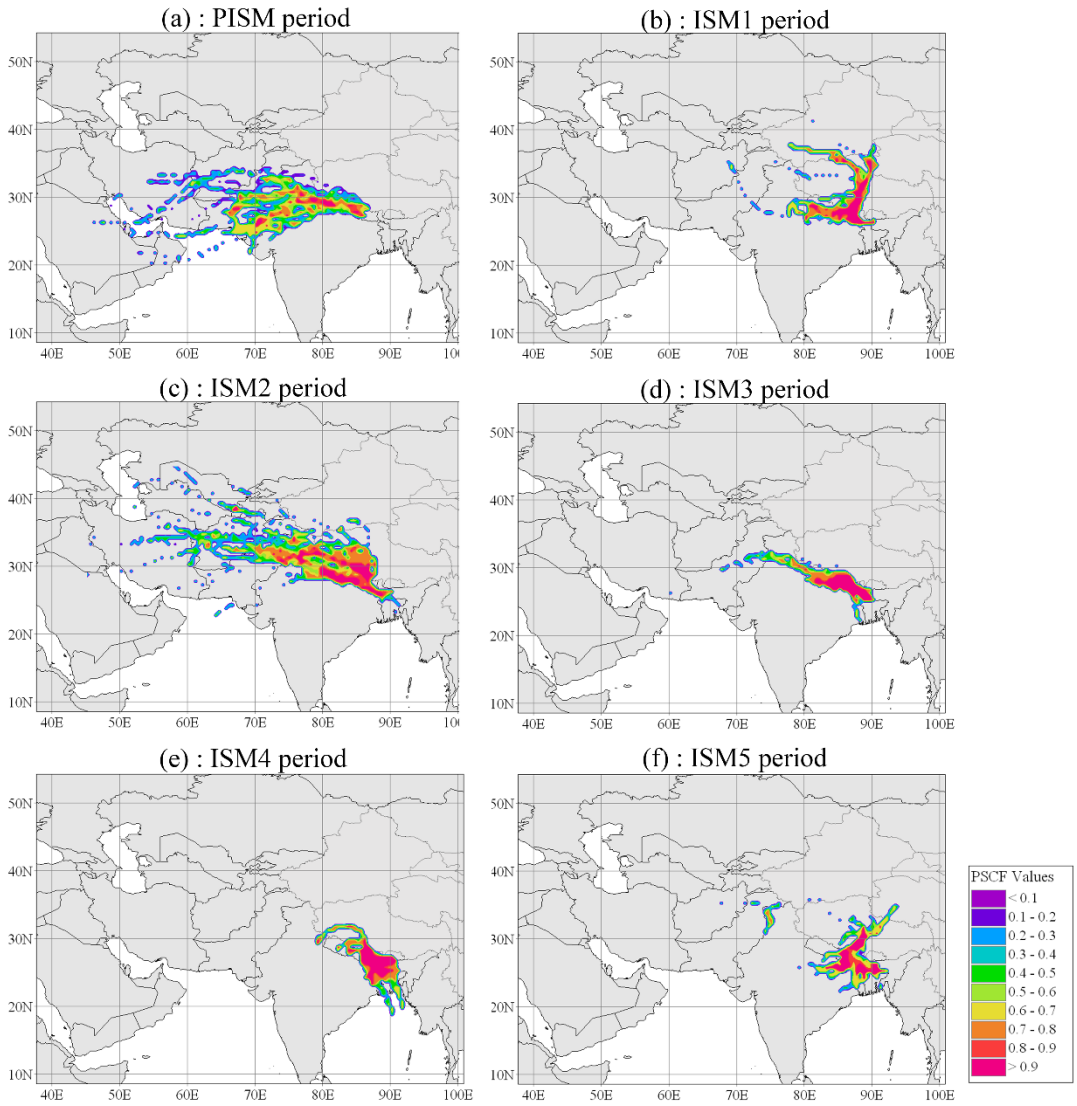
(a) : PISM period
(b) : ISM1 period
(c) : ISM2 period
(d) : ISM3 period
(e) : ISM4 period
(f) : ISM5 period
50N
40N
30N
20N
10N
40E
50E
60E
70E
80E
90E
100E
PSCF Values
< 0.1
0.1 - 0.2
0.2 - 0.3
0.3 - 0.4
0.4 - 0.5
0.5 - 0.6
0.6 - 0.7
0.7 - 0.8
0.8 - 0.9
> 0.9

Figure 7

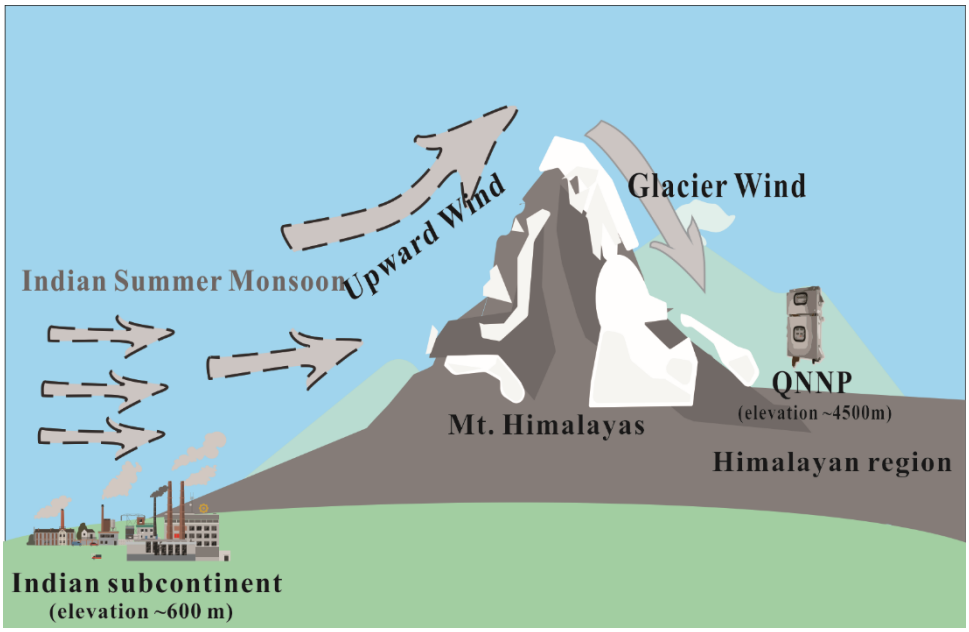
Upward Wind
Glacier Wind
Indian Summer Monsoon
QNNP
(elevation ~4500m)
Mt. Himalayas
Himalayan region
Indian subcontinent
(elevation ~600 m)

933

934 **Table 1. Statistical metrics of GEM, GOM, PBM and meteorological variables at the**

935 **Qomolangma National Nature Preserve**

Period	Statistical	T (℃)	RH(%)	WS(m s^{-1})	GEM (ng m^{-3})	GOM (pg m^{-3})	PBM (pg m^{-3})
PISM	Minimum	-5.6	1	0	0.54	11.9	9.8
	1st Qu.	1.6	11	1.8	0.99	21.7	22.3
	Median	6.4	25	3.6	1.19	29.5	26.8
	Mean	6.1	33	4.1	1.31	35.2	30.4
	3rd Qu.	11.2	53	6.3	1.58	42.8	36.0
	Maximum	16.3	89	13.9	2.91	101.3	92.6
ISM1	Min	-3.8	9	0	0.15	7.5	9.5
	1st Qu.	1.6	33	1.3	1.20	15.2	17.0
	Median	5.6	49	2.2	1.38	19.2	19.2
	Mean	5.6	50	2.7	1.44	20.3	21.2
	3rd Qu.	9.8	65	3.6	1.63	24.1	24.5
	Max	15.7	91	10.3	2.74	64.0	59.1
ISM2	Min	-1.3	3	0	0.47	4.4	12.7
	1st Qu.	4.1	30	1.3	1.14	18.6	40.4
	Median	8.5	48	2.2	1.35	23.9	54.8
	Mean	8.8	46	3.0	1.45	25.5	53.4
	3rd Qu.	13.7	64	4	1.68	31.3	64.9
	Max	19.6	87	11.2	3.74	63.4	106.3
ISM3	Min	2.6	26	0	0.78	3.6	1.1
	1st Qu.	8.1	44	1.3	1.33	14.7	12.7
	Median	11.8	58	2.7	1.51	19.0	17.2
	Mean	12.0	58	2.9	1.56	19.3	16.9
	3rd Qu.	15.6	73	4	1.72	23.3	21.3
	Max	21.8	92	9.9	2.70	36.6	31.3
ISM4	Min	6.0	25	0	0.66	7.1	0.5
	1st Qu.	9.3	43	1.3	1.35	13.2	10.9
	Median	12.1	61	2.7	1.46	18.1	17.4
	Mean	13.0	58	2.9	1.51	21.1	20.0
	3rd Qu.	16.6	72	3.6	1.61	24.9	26.1
	Max	22.7	90	9.9	2.62	149.1	78.6
ISM5	Min	2.2	18	0	0.48	1.1	0.3
	1st Qu.	8.3	59	0.9	1.17	7.6	6.6
	Median	10.7	75	2.2	1.35	11.0	9.8
	Mean	11.4	72	2.3	1.32	12.6	11.0
	3rd Qu.	14.1	86	3.1	1.49	16.2	14.3
	Max	22.9	96	9.4	2.45	121.3	33.2

936

937
938 **Table 2. Comparison of atmospheric Hg concentrations and diurnal variation of GEM at QNNP with measurements from previous studies**
939

Location	Elevation	Classification	Time period	GEM/(*TGM*)	GOM	PBM	GEM diurnal variation (Local time/GEM Conc.)			reference
				(ng m^{-3})	(pg m^{-3})	(pg m^{-3})	peak	valley	variation value	
Mt. Waliguan, China	3816	remote	Sep 2007-Sep 2008	*(1.98±0.98)*	7.4±4.8	19.4±18.1	6/2.3	14/1.94	0.36	(Fu et al., 2012a)
Mt. Leigong, China	2178	remote	May 2008-May 2009	2.80±1.51	-	-	14/2.99	5/2.52	0.47	(Fu et al., 2010)
Mt. Gongga, China	1640	remote	May 2005-July 2006	*(3.98)*	-	-	11/4.45	2/3.55	0.90	(Fu et al., 2008)
Kodaikanal, India	2343	rural	Nov 2012-Sep 2013	*(1.53±0.21)*	-	-	16/1.66	7/1.43	0.23	(Karthik et al., 2017)
EvK2CNR, Nepal	5050	remote	Nov 2011-Apr 2012	*(1.2±0.2)*			18/1.3	6/1.1	0.1	(Gratz et al., 2013)
Shangri-La, China	3580	remote	Nov 2009-Nov 2010	*(2.51±0.73)*	8.22±7.9	38.32±31.26	17/2.48	6/1.71	0.77	(Zhang et al., 2015a)
Miyun, China	220	rural	Dec 2008-Nov 2009	3.22±1.74	10.1±18.8	98.2±112.7	20/3.40	10/3.00	0.40	(Zhang et al., 2013)
Penghu Islands, China	25	coastal	Mar 2011-Jan 2012	*(3.17±1.17)*	-	-	11/3.48	1/2.87	0.61	(Jen et al., 2014)
Shanghai, China	17	Urban	Jun 2014–Dec 2014	4.19±9.13	21±100	197±877				(Duan et al., 2017)
Namco, China	5300	remote	Nov 2014-Mar 2015	1.33±0.24	-	-				(Yin et al., 2018)
ALS, China	2450	remote	May 2011-May 2012	*(2.09±0.63)*	2.3±2.3	31.3±28.4	-	-	-	(Feng and Fu, 2016)
QNNP, China (this study)	4267	remote	Apr 2016-Aug 2016	1.42±0.37	21.4±13.4	25.6±19.1	6/2.04	13/1.11	0.93	This study

940
941